

FORWARD PHYSICS OF HADRONIC COLLIDERS

*I. P. Ivanov*¹

IFPA, University of Liege, Liege, Belgium,
Sobolev Institute of Mathematics, Novosibirsk, Russia

These lectures were given at the Baikal Summer School on Physics of Elementary Particles and Astrophysics in July 2012. They can be viewed as a concise introduction to hadronic diffraction, to the physics of the pomeron and related topics.

Эти лекции, прочитанные на Байкальской летней школе по физике элементарных частиц и астрофизике в 2012 г., могут рассматриваться как краткое введение в физику адронной фракции, померона и связанных с ними вопросов.

PACS: 13.85.Lg; 13.85.Dz; 12.40.Nn

INTRODUCTION

The main focus of the experiments at high-energy hadronic colliders, such as Tevatron and the LHC, lies in and beyond the Standard Model of the electroweak physics. In order to produce heavy particles, experimentalists smash protons and select hard collision events, which are initiated by large-angle scattering of individual quarks and gluons. The protons, of course, are completely disintegrated in this scattering, and the invariant mass of the remnants of each initial proton is very large.

However, there exists another class of hadronic processes at very high energies, which are very rich and remarkably different from hard collisions. The main feature of these reactions is that the initial protons remain intact or «almost intact»; that is, they are excited into a hadronic system of rather small invariant mass, much smaller than the collision energy. These are often called semihard reactions, or diffractive processes, or simply *hadronic diffraction*. The experimental signature of diffraction is that all hadrons are produced at small angles, close to the forward direction, hence the name «forward physics».

Diffractive processes tell us a lot about the complicated structure of hadrons, which is one of the main research objects in modern particle physics. For a theorist, it has additional flair because, rather surprisingly, it is the place where a vast range of theoretical approaches can grasp some part of reality. These approaches span from purely phenomenological Regge-theory-inspired models and all the way up to the rigorous perturbative QCD and even to the gauge-string duality [1]. It is therefore an ideal sandbox for models or approaches which attempt to interpolate between soft and hard regimes of strong interactions.

¹E-mail: Igor.Ivanov@ulg.ac.be

The history of the subject is very long, and it continues to be written today as the LHC experiments publish their data on various diffractive processes. In these introductory lectures we offer a glimpse into a variety of diffraction-related topics, trying to cover theory, phenomenology and experiment in 20 pages. Much more detailed and in-depth reviews can be found in [2,3]. There also exist two series of topical workshops called «Diffraction» and «Low- x », whose proceedings will provide the interested reader with all the details.

1. FORWARD PHYSICS AND DIFFRACTION

1.1. Rapidity-Angle Diagram. Let us start with simple kinematical considerations. Each particle produced in a collision process flies away in a direction defined by its polar angle θ and azimuthal angle ϕ . In hadronic collisions, one usually uses *pseudorapidity* $\eta = -\ln \tan(\theta/2)$ instead of θ itself. It carries the prefix «pseudo» because at high energies it is very close but not exactly equal to the true rapidity, the additive kinematical quantity defined as $0.5 \ln((E + p_z)/(E - p_z))$. Thus, angular distributions of the final system produced at hadronic colliders is described in the (pseudo)rapidity-(azimuthal) angle diagram.

The reason for choosing pseudorapidity instead of θ is that a typical multihadron final state would be strongly peaked near the forward and backward directions if plotted against θ , while it is distributed more or less homogeneously in the rapidity-angle diagram, see Fig. 1, top row. Qualitatively, this happens because collision of two energetic protons leads to production of many «soft» hadrons whose transverse momenta are rather small, within 1 GeV or so, while

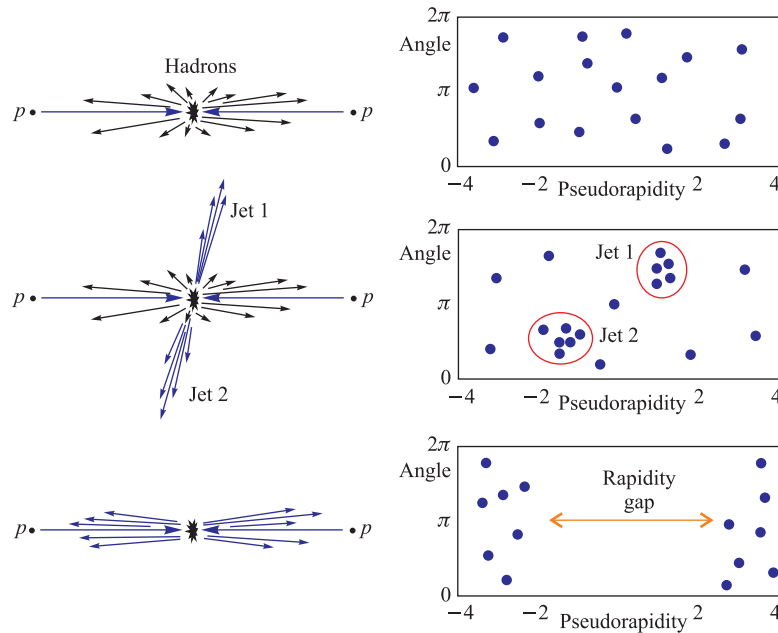


Fig. 1. Typical processes at high-energy hadronic colliders and their representation in the rapidity-angle diagram

their longitudinal momenta can be a sizable fraction of the initial proton's momentum. In experimentalist's language, these are called «minimum bias events».

There is, of course, a significant percentage of processes in which a truly hard partonic scattering happens. It leads to production of two or more *hadronic jets*, collimated flows of energetic hadrons. Jets appear as compact clusters on the pseudorapidity-angle diagram, Fig. 1, middle row, but still they stand on the pedestal of soft hadrons filling the diagram.

Quite often one sees a remarkable type of processes with large regions completely void of particles, Fig. 1, bottom row. These empty regions are called *rapidity gaps*, and they can extend to several units of rapidity. The ultimate form of these rapidity gap events is elastic pp or $p\bar{p}$ scattering, in which protons survive and just get deflected by a small angle. Plotted on the rapidity-angle diagram, they will look like two points at the opposite ends of the diagram with an empty region of 10 units in rapidity or so.

Presence of these rapidity gap events poses a challenge. They cannot happen by chance: with many dozens of hadrons scattered across the diagram, the probability of making a sizable gap purely by chance is nowhere near the observed fraction of such events. Moreover, at the LHC energies, $E_p = 4$ TeV, the elastic proton scattering can seem almost miraculous: the proton is so fragile that even a tiny fraction of this energy would be enough to break it into a splash of hadrons.

The only way out is to admit that a novel mechanism responsible for rapidity-gap events must be at work. This mechanism must be (1) driven by strong interactions, (2) does not have to change the quantum numbers of particles, (3) it must persist at high energies. We can picture this mechanism as a t -channel exchange of a novel dynamical QCD object, which is known as pomeron (the Pomeranchuk singularity). «Hadronic diffraction» and «forward physics» are two roughly equivalent umbrella terms for rapidity gap events and the physics of the pomeron exchange.

1.2. Diffractive Scattering in Quantum Mechanics. In order to get the first peek into the physics of hadronic diffraction, let us start with the usual quantum mechanical scattering off a central potential. Since the orbital angular momentum is conserved in this scattering, we have the standard partial wave representation of the elastic scattering amplitude:

$$f(\theta) = \frac{1}{2ik} \sum_{\ell} (2\ell + 1)(S_{\ell} - 1)P_{\ell}(\cos \theta). \quad (1)$$

The strength of the scattering in a given partial wave is encoded in the scattering matrix element S_{ℓ} ; having $S_{\ell} = 1$ means no scattering in this partial wave. This expression can be used to calculate the elastic cross section,

$$\sigma_{\text{el}} = \int d\Omega |f(\theta)|^2 = \frac{\pi}{k^2} \sum_{\ell} (2\ell + 1) |1 - S_{\ell}|^2, \quad (2)$$

and, via optical theorem, the total cross section:

$$\sigma_{\text{tot}} = \frac{4\pi}{k} \text{Im} f(\theta = 0) = \frac{\pi}{k^2} \sum_{\ell} (2\ell + 1) 2(1 - \text{Re} S_{\ell}). \quad (3)$$

The inelastic scattering, the difference between the two, can then be written as

$$\sigma_{\text{inel}} = \sigma_{\text{tot}} - \sigma_{\text{el}} = \frac{\pi}{k^2} \sum_{\ell} (2\ell + 1) (1 - |S_{\ell}|^2). \quad (4)$$

In a purely elastic scattering, $|S_\ell| = 1$, so that the outgoing flux is equal to the incoming flux in each partial wave. However, in the opposite case of perfectly absorbing center («black sphere») something interesting happens. Here we have zero outgoing flux for partial waves that fall on the center: $S_\ell = 0$ for some ℓ . Within each of these partial waves, we get

$$\sigma_{\text{el}}^{(\ell)} = \sigma_{\text{inel}}^{(\ell)} = \frac{1}{2}\sigma_{\text{tot}}^{(\ell)}. \quad (5)$$

In other words, despite absence of outgoing waves, we still have scattering in these partial waves!

This scattering is due to diffraction. A portion of the incoming wave which is completely blocked by the absorber disappears, the transmitted wave «feels» this gap and begins to distort its wave front, closing the gap. Asymptotically, these distorted wave fronts appear as scattered waves.

It is useful to view diffraction as the process of «actualizing» hidden degrees of freedom. Although the initial plane wave propagates in a well-defined direction, it contains in fact many incoming and outgoing waves, which add up just in the right way. These are the hidden degrees of freedom which are perfectly balanced in the plane wave. Absorption breaks this balance, making these degrees of freedom observable and leading to elastic scattering at nonzero angles.

Optical diffraction of white light represents yet another form of this effect. All colors add up to white light in the incoming wave, but they become imbalanced upon diffraction. The resulting colored diffraction peaks are the manifestation of how the hidden color degree of freedom is actualized.

The elastic scattering due to diffraction is unique in its ability to preserve a fragile system. Even if the incoming wave corresponds to composite system with tiniest break-up energy, diffraction still manages to deflect this system by acting coherently on its constituents. This picture should explain why hadronic diffraction is the ideal candidate for rapidity gap events, in which fragile systems (protons) are slightly deflected but not destroyed.

1.3. Diffractive Scattering of Hadrons. The high-energy QCD is a theory of quarks and gluons. Is there a room for the pomeron exchange in it? If so, how does it arise?

There are features of the QCD pomeron which can be deduced on general grounds. First, it must involve gluons. Indeed, it is a general result in field theory that the exchange of a fundamental particle with spin j leads, at the tree level, to the energy behavior of the cross section $\sigma \propto s^{2(j-1)}$. Since elastic and diffractive scattering cross sections do not decrease with energy, it is natural to expect that spin-1 particles (that is, gluons) are the main building blocks of the pomeron. Second, gluons carry color, while the pomeron exchange is colorless. Therefore, the pomeron must involve at least two gluons in the t -channel in the color singlet state. This very simplified model can already be used for rough estimates.

Upon a second thought, one can realize that the physics of the pomeron must be way more complicated than this two-gluon-exchange picture. Indeed, this picture would lead to cross sections which are exactly constant with energy. However, the total, elastic and diffractive hadronic cross sections measured experimentally exhibit in fact a slow rise with energy growth. For example, if the total pp cross section is parametrized at high energy by a power law $\sigma_{\text{tot}} \propto s^\delta$, then the fit yields $\delta \approx 0.1$.

This rise on its own could be well accommodated within the Regge picture, if the exponent δ were constant. In reality it is not. The value of δ seems to depend on the «hardness»

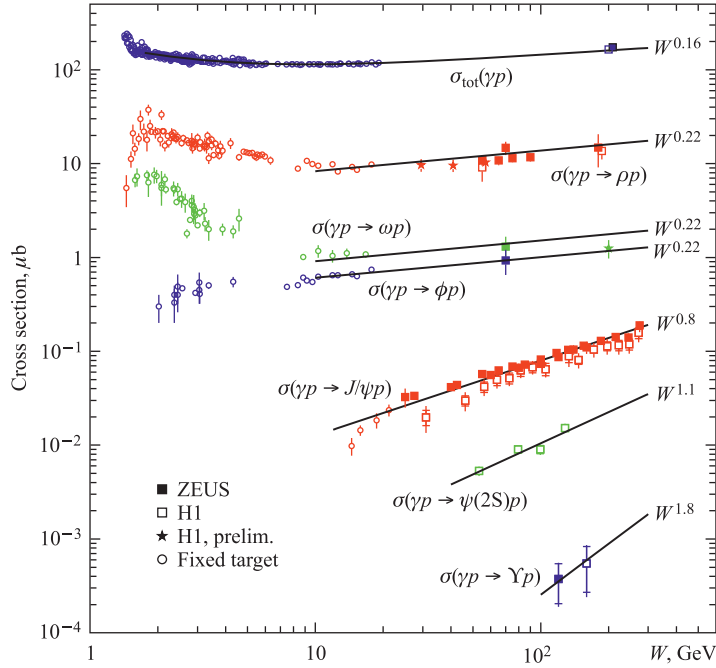


Fig. 2. Energy behaviour of the diffractive vector meson photoproduction cross section for different vector mesons

of the effective pomeron-projectile vertex. One impressive example is diffractive vector meson photoproduction, $\gamma p \rightarrow Vp$, where V stands for any neutral vector meson: $V = \rho, \omega, \phi, J/\psi, \Upsilon$ or their excited states, see review [6]. The energy dependence of this process was well measured at the electron–proton collider HERA and in fixed target experiments, see Fig. 2. The value of δ steadily increases with the mass of the meson from 0.22 for ρ to 1.6 for Υ ; the harder the process, the larger is δ . Describing this broad region where δ can vary represents a challenge for the Regge picture of the pomeron.

There are also purely theoretical issues to be concerned about. First, it would be nice to see directly how a powerlike behavior with a small δ appears from the diagram calculations. If we imagine that the two t -channel gluons are the first approximation and then take into account gluon interactions, we will get multiloop diagrams, which typically give us only logarithms of energy. Next, even if we manage to derive the powerlike behavior, we run into troubles with the Froissart bound which says that asymptotically cross section cannot grow faster than $\log^2 s$. This means that at sufficiently high energy the powerlike growth must flatten due to some nonlinear evolution mechanism. The challenge is to derive this mechanism from the first principles in QCD.

1.4. Small-Angle Elastic pp Scattering as the Simplest Diffractive Process. Perhaps, the simplest example of hadronic diffraction is the high-energy elastic pp (or $p\bar{p}$) scattering at very small angles (for a much deeper review, see [3]). Depending on the value of the momentum transfer squared, $|t|$, it proceeds in different regimes (Fig. 3):

- At $|t|$ of the order of 1 GeV^2 or smaller, it displays hallmark features of diffractive scattering. These are, first, the pronounced *diffraction cone*, that is, approximately exponential

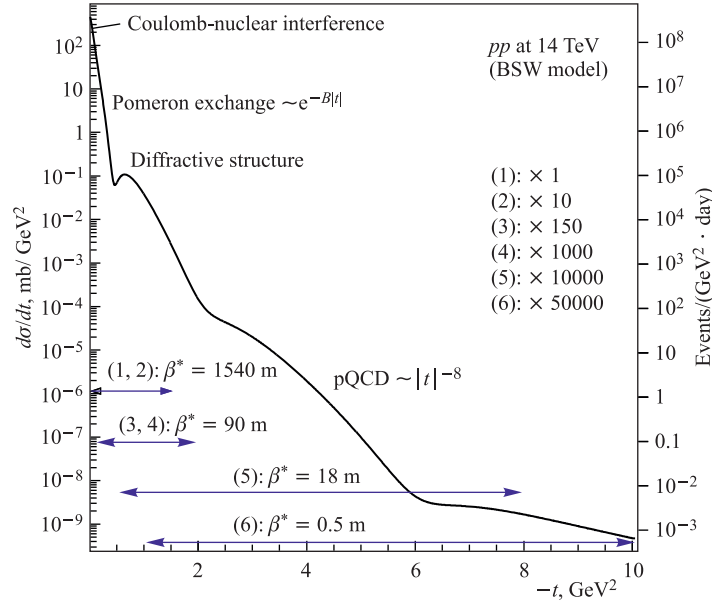


Fig. 3. Elastic pp scattering at the LHC energies in different $|t|$ -regions. Shown are predictions for the LHC from the BSW model [7]

dependence of the cross section on the momentum transfer, $d\sigma/d|t| \propto \exp(-B_{\text{el}}|t|)$, where the parameter B_{el} is called the (elastic) slope of diffraction cone, and, second, the presence of diffractive dips and bumps in the angular distribution. In this region the true quantum-mechanical proton diffraction takes place: two colliding protons are opaque, they partially block each other and, consequently, diffract.

- At much larger values of $|t|$, the process becomes harder, so that the perturbative QCD becomes applicable, and the scattering proceeds via moderate or large angle coordinated deflection of individual valence quarks by hard gluon exchanges.

- The Coulomb scattering amplitude due to electromagnetic interaction must be included in the full description, and at very small t , well below 0.01 GeV^2 , it dominates over hadronic scattering.

It is important to mention that the hadronic scattering amplitude in the strictly forward case ($|t| = 0$) is a very important quantity because its imaginary part determines, via the optical theorem, the total cross section of the process $pp \rightarrow \text{hadrons}$. One can therefore say that the total pp scattering also belongs to the field of diffraction, despite the fact that individual channels have physics very different from diffraction.

In the diffractive region, the intensity of diffraction is related to the «opacity» of the proton. This opacity is a nonperturbative quantity, so it can be calculated only within some models. However, there is a standard way to link this opacity, or the profile function, to the scattering cross section, which we now expose.

This method is a slight adaptation of the quantum-mechanical diffractive scattering described above. That method was based on partial wave expansion, which is a good expansion basis for low-energy scattering, in which the wavelength is comparable or larger than the size

of the scatterer. In the opposite situation, that is, at high energies, there are many partial waves which are blocked by the absorbed. Quasiclassically, a partial wave with the orbital quantum number ℓ corresponds to the typical impact parameter $b \sim \hbar\ell/p$. If the scatterer is large, $R \gg \lambda$, we get $\ell \gg 1$. So, instead of partial wave expansion we can use another basis: impact parameters expansion, in which we describe scattering in terms of two-dimensional impact parameter \mathbf{b} between the centers of the two colliding protons. Its conjugate variable is \mathbf{q} , the transverse momentum transfer, and the quantum-mechanical scattering amplitude can be written, instead of partial wave expansion, as

$$f(\theta) = \frac{1}{(2\pi)^2} \int d^2\mathbf{b} e^{i\mathbf{q}\mathbf{b}} f(\mathbf{b}). \quad (6)$$

Switching from the quantum-mechanical to quantum-field-theoretical description of the scattering process, we introduce the (diagonal) scattering matrix in the \mathbf{b} -space, $S(\mathbf{b})\langle pp|\hat{S}|pp\rangle$. It is diagonal because at very high energies, there is strong time dilatation for the protons, and the interaction is so quick that the proton's centers of mass have no time to shift.

Then, as usual, we write the S -matrix as $1 + ia(s, \mathbf{b})$, where $a(s, \mathbf{b})$ is the profile function describing the opacity of the proton. The differential cross section becomes

$$\frac{d\sigma_{\text{el}}}{d|t|} = \frac{|\mathcal{M}(s, t)|^2}{16\pi s^2}, \quad \text{where } \mathcal{M}(s, t) = 2s \int d^2\mathbf{b} e^{i\mathbf{b}\mathbf{q}} a(s, \mathbf{b}). \quad (7)$$

One can then find that

$$\sigma_{\text{el}} = \int d^2\mathbf{b} |a(s, \mathbf{b})|^2, \quad \sigma_{\text{tot}} = 2 \int d^2\mathbf{b} \text{Im } a(s, \mathbf{b}). \quad (8)$$

Now comes the modeling. Since the pomeron exchange is short-ranged, $a(s, \mathbf{b})$ has a compact shape with typical size of $\sim 2R_p$, the proton diameter. Also, a is mostly imaginary. So it can be phenomenologically parametrized in the first approximation as

$$a(s, \mathbf{b}) = ia_0(s) \exp\left(-\frac{\mathbf{b}^2}{2B_{\text{el}}}\right), \quad (9)$$

where we expect $B_{\text{el}} \sim R_p^2 \sim 1 \text{ fm}^2 \approx 25 \text{ GeV}^{-2}$. Then we get

$$\frac{d\sigma_{\text{el}}}{d|t|} = \pi B_{\text{el}}^2 a_0^2 e^{-B_{\text{el}}|t|}, \quad \sigma_{\text{el}} = \pi B_{\text{el}} a_0^2. \quad (10)$$

This gives a hint how an approximate exponential dependence comes about from a compact profile function. Also, the slope B_{el} is clearly related with the size of the proton, and therefore it cannot be calculated from pQCD. But it can be found from a fit to the experimental data; a fit to the Tevatron data gives

$$B_{\text{el}} \approx 17 \text{ GeV}^{-2}, \quad a_0 = 0.974 \pm 0.042.$$

The diffraction slope roughly agrees with the expectations.

The fact that a_0 is close to 1 means that the proton (at the TeV energies) is indeed very opaque, at least near its center. This is usually formulated as the pp scattering approaching the black disc limit in the head-on collision. Indeed, $S(\mathbf{b} = 0) = 1 + ia(\mathbf{b} = 0) = 1 - a_0 \ll 1$. This conclusion has very important implications for the partonic structure of the proton, the evolution and saturation of partonic densities, etc. This is one of the many examples of interplay between nonperturbative and perturbative physics which arise in diffractive scattering.

2. EXPERIMENTAL ISSUES

Studying rapidity gap processes at hadronic colliders is a challenging business, and it becomes even harder with the energy growth. The main problem can be seen from kinematics. If typical transverse momenta of diffractively produced particles are of order 100 MeV, while the longitudinal momenta at the LHC are $\approx E_p = 4$ TeV, then the typical scattering angle is of the order of one arcminute or less. Such particles cannot be observed by the main detectors simply because they do not leave the vacuum pipe on the detector scales. In fact, the situation is worse because these scattered particles do not even leave the parent *beam* over long distances. Therefore, studying diffraction immediately imposes specific requirements on instrumentation, both on the accelerator and detector side.

2.1. Roman Pot Detectors. A proton which is scattered elastically at the LHC and which gains the transverse momentum of 100 MeV, leaves the beam only several dozen meters downstream. If would leave the beam pipe kilometers downstream, and therefore tracking this proton with the conventional detectors becomes impossible. The idea, which goes back to the 1970s, is to construct very small detectors and put them *inside* the vacuum pipe. Detectors of this type are called *Roman Pots*. They are movable: one should be able to approach the beam as close as possible, ideally within several millimeters, but at the same time one should be able to retract them in safe position at the stages when the beam is not yet safe (when it is injected, accelerated, and squeezed). Roman Pots are implemented in one of the LHC experiments, TOTEM [4], and other similar detectors are also being developed (for example, the FP420 project [5]).

In Fig. 4 we show a Roman Pot station of TOTEM, one of the seven experiments working at the LHC, and its plate with the pixel detector. Note the unusual shape of the detector: it has a naked sensitive edge with no dead material which allows it to approach the beam as close as possible.

One additional remarkable thing about the Roman Pot detectors is that they can detect protons which are scattered at exactly zero angle, provided that they lose about 1% of their energy at the collision. We leave it as a simple exercise to the reader to determine at what distance downstream one must place a Roman Pot detector to achieve this feat.

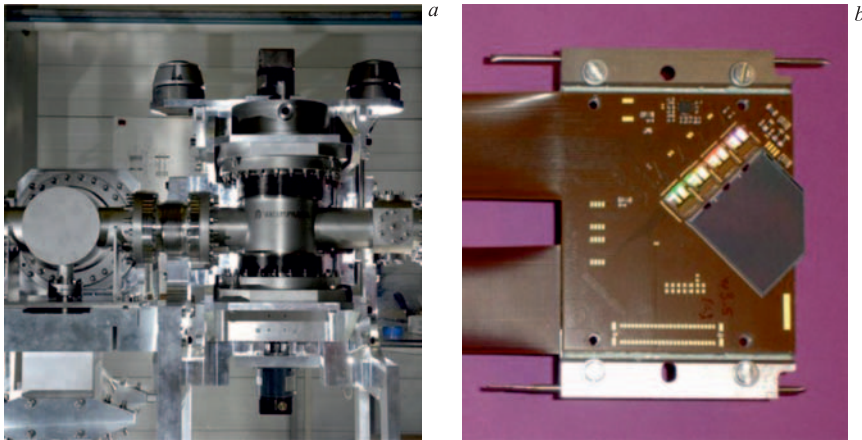


Fig. 4. Roman Pot station of TOTEM [4] (a) and one of the pixel detector plates used in it (b)

2.2. Large- β^* Beams. The proton beams are strongly focused by quadrupole magnets just before the collision points. This is done to achieve the highest particle density at the point of bunch crossing and reach the highest luminosity. As a result, the beams have an intrinsic angular spread. If a proton is scattered by an angle smaller than this spread, it will stay inside the beam and will never be detected.

The way out of this difficulty is to *defocus* beams, reducing their intrinsic angular spread and making them as parallel as possible. This will, of course, strongly reduce the luminosity, but since all diffractive cross sections are large, it will not be a problem for the event rate.

Focusing of the beams are usually characterized by the value of β^* , which is the distance downstream from the focusing point where the beam geometric cross section becomes twice larger. The tighter the focusing, the smaller is β^* . The nominal value at the LHC is $\beta^* = 0.55$ m. During special runs dedicated to forward physics, the beams are brought into configuration with $\beta^* = 90$ m and even up to 1.54 km. These special runs are very short but they are foreseen by the LHC schedule. Figure 3 shows, among other, which t -regions in the elastic pp scattering at the LHC can be probed with various β^* -configurations.

2.3. Coping with the Pile-Up. Yet another problem concerns attributing the protons detected in the Roman Pot to a specific hard collision. At the LHC, each beam crossing results in several or even several dozens of individual proton–proton scatterings. Each of them produces lots of tracks, see Fig. 5, which are recorded by the main detector. In addition, there might be a signal coming from the Roman Pots placed at hundreds of meters away of a proton deflected by a small angle. This proton must originate from one of these individual primary vertices, but from which one?

The only way to find it is to measure the timing of the proton detection in Roman Pots with sufficient precision. The goal here is to reach 10 ps accuracy, which will allow one to distinguish vertices several millimeters apart. Unfortunately, this goal is not yet reached, but experimentalists keep working on this issue.

Luckily, the pile-up is not an issue in the large- β^* configuration. Nevertheless, there are specific processes such as central exclusive Higgs production [8], which have very small cross section and must be studied with tightest focusing possible. Then, achieving good timing resolution becomes a must.

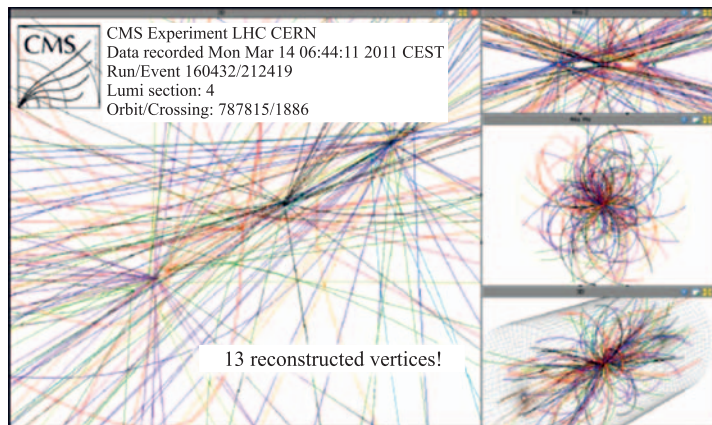


Fig. 5. Illustration of the pile-up: this multiparticle event has 13 reconstructed primary vertices corresponding to independent individual pp scattering events in a single bunch crossing

3. POMERON IN A TOY MODEL

As mentioned above, the powerlike energy behavior of the cross section with a small non-integer exponent looks somewhat strange because loop diagrams usually produce logarithms of energies. However, it turns out that when all diagrams are resummed in the leading logarithmic approximation, such a power law can arise.

This is exactly what happens in QCD for the quark and gluon exchanges and is known as *reggeization* of the quark and gluon. For the pomeron, the situation in the real QCD is not that simple, but the series of the loop diagrams can still be resummed. In this section we will illustrate how such a resummation can work in a very simple toy model, which is taken from the book [10] with some further simplifications.

Consider a theory with massless scalar «quarks» and massive scalar «gluons» with mass m which interact via trilinear vertices with equal couplings mg (m is introduced into trilinear coupling to make g dimensionless). For calculational simplicity, we also suppress the color degree of freedom, which plays important role in the true QCD.

Consider now the imaginary part of the high-energy elastic «quark–quark» scattering at nonzero t . We want to recover the powerlike behavior

$$\text{Im } \mathcal{M}(s, t) \propto s^{\alpha_P(t)}, \quad (11)$$

and find the value of the pomeron intercept $\alpha_P(t)$.

3.1. One-Loop Result. The one-gluon exchange diagrams give a purely real amplitude; therefore, we start with the one-loop two-gluon-exchange diagrams (we disregard annihilation diagrams because they contain quarks in the t -channel which are suppressed in true QCD). At this order, we have two diagrams shown in Fig. 6. One can check that the nonplanar diagram does not have the imaginary part due to kinematics, so we focus on the box diagram only.

The imaginary part at the 1-loop level can be calculated by applying Cutkosky's rules, which are a generalization of the optical theorem:

$$\text{Im } \mathcal{M}^{(1)} = \frac{1}{2} \int dF_2 \mathcal{A}_{2 \rightarrow 2}(k) \mathcal{A}_{2 \rightarrow 2}^\dagger(k - q), \quad (12)$$

where dF_2 is the two-particle phase space,

$$dF_2 = \frac{d^4 \ell_1}{(2\pi)^3} \delta(\ell_1^2) \frac{d^4 \ell_2}{(2\pi)^3} \delta(\ell_2^2) (2\pi)^4 \delta^{(4)}(p_1 + p_2 - \ell_1 - \ell_2), \quad (13)$$

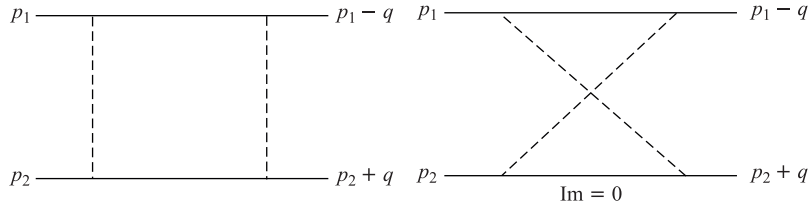


Fig. 6. One-loop diagrams for qq scattering in the toy model; only the planar box diagram gives contribution to the imaginary part of the amplitude

while $\mathcal{A}_{2 \rightarrow 2}$ is the tree-level $2 \rightarrow 2$ scattering amplitude,

$$\mathcal{A}_{2 \rightarrow 2}(k) = \frac{m^2 g^2}{k^2 - m^2 + i\epsilon}. \quad (14)$$

One integration in (12) can be immediately done, giving

$$\text{Im } \mathcal{M}^{(1)} = \frac{1}{8\pi^2} \int d^4 k \delta[(p_1 - k)^2] \delta[(p_2 + k)^2] \frac{m^4 g^4}{(k^2 - m^2)((k - q)^2 - m^2)}. \quad (15)$$

It is now convenient to use Sudakov variables. In the center of motion frame we write

$$p_1^\mu = \frac{\sqrt{s}}{2}(1, 0, 0, 1), \quad p_2^\mu = \frac{\sqrt{s}}{2}(1, 0, 0, -1), \quad (16)$$

so that $p_1^2 = 0 = p_2^2$, $(p_1 + p_2)^2 = 2p_1 p_2 = s$. Then the «gluon» momentum is parametrized as $k^\mu = \alpha p_1^\mu - \beta p_2^\mu + k_\perp^\mu$ and $d^4 k = -(s/2) d\alpha d\beta d^2 \mathbf{k}$, where \mathbf{k} is the 2D transverse momentum. The two delta-functions then become $\delta[\beta(1 - \alpha)s - \mathbf{k}^2]$ and $\delta[\alpha(1 - \beta)s - \mathbf{k}^2]$. An important observation is then that typical $\mathbf{k}^2 \ll s$, so that $\alpha = \beta \approx \mathbf{k}^2/s \ll 1$. Therefore,

$$\int d\alpha d\beta \delta[(p_1 - k)^2] \delta[(p_2 + k)^2] \approx \int d\alpha d\beta \delta(\beta s - \mathbf{k}^2) \delta(\alpha s - \mathbf{k}^2) = \frac{1}{s^2}.$$

Also, $k^2 = -\alpha\beta s - \mathbf{k}^2 \approx -\mathbf{k}^2$ and $(k - q)^2 \approx -(\mathbf{k} - \mathbf{q})^2$. Bringing all coefficients together, we finally get the one-loop result:

$$\text{Im } \mathcal{M}^{(1)} = \frac{m^4 g^4}{16\pi^2 s} \int \frac{d^2 \mathbf{k}}{(\mathbf{k}^2 + m^2)((\mathbf{k} - \mathbf{q})^2 + m^2)}. \quad (17)$$

Note that at this level, the intercept $\alpha_P = -1$ is an integer number and is consistent with the fact that we have scalar particles exchanged in the t -channel.

3.2. Two-Loop Result. We start the analysis of the two-loop contribution with the ladder diagram shown in Fig. 7. Again, by Cutkosky's rules, we get

$$\text{Im } \mathcal{M}^{(2)} = \frac{1}{2} \int dF_3 \mathcal{A}_{2 \rightarrow 3}(k_1, k_2) \mathcal{A}_{2 \rightarrow 3}^\dagger(k_1 - q, k_2 - q), \quad (18)$$

where dF_3 is the three-particle phase space,

$$dF_3 = \frac{d^4 \ell_1}{(2\pi)^3} \delta(\ell_1^2) \frac{d^4 \ell_2}{(2\pi)^3} \delta(\ell_2^2) \frac{d^4 \ell_3}{(2\pi)^3} \delta(\ell_3^2) (2\pi)^4 \delta^{(4)}(p_1 + p_2 - \ell_1 - \ell_2 - \ell_3),$$

and $\mathcal{A}_{2 \rightarrow 3}$ is $2 \rightarrow 3$ tree-level scattering amplitude,

$$\mathcal{A}_{2 \rightarrow 3}(k_1, k_2) = \frac{m^6 g^6}{(k_1^2 - m^2)(k_2^2 - m^2)}. \quad (19)$$

Consider first the longitudinal integral $\int d\alpha_1 d\beta_1 d\alpha_2 d\beta_2 \delta(\ell_1^2) \delta(\ell_2^2) \delta(\ell_3^2)$. Using Sudakov variables, $k_i = \alpha_i p_1 - \beta_i p_2 + k_{i\perp}$, we get

$$\begin{aligned} \ell_1^2 &= (1 - \alpha_1)\beta_1 s - \mathbf{k}_1^2, \\ \ell_2^2 &= (\alpha_1 - \alpha_2)(\beta_2 - \beta_1)s - (\mathbf{k}_1 - \mathbf{k}_2)^2 = 0, \\ \ell_3^2 &= (1 - \beta_2)\alpha_2 s - \mathbf{k}_2^2 = 0. \end{aligned} \quad (20)$$

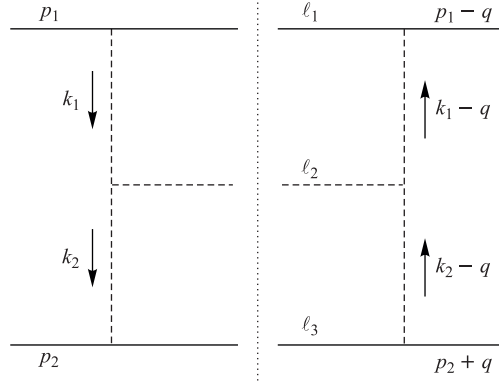


Fig. 7. The only two-loop diagram contributing to the imaginary part in the leading logarithmic approximation

Then in the remaining integration we note that there is a logarithmically enhanced contribution from the region

$$1 \gg \alpha_1 \gg \alpha_2 \approx \frac{\mathbf{k}_2^2}{s}, \quad \frac{\mathbf{k}_1^2}{s} \approx \beta_1 \ll \beta_2 \ll 1, \quad \alpha_1 \beta_2 = \frac{(\mathbf{k}_1 - \mathbf{k}_2)^2}{s}, \quad (21)$$

and the longitudinal integral becomes

$$\frac{1}{s^2} \int d\alpha_1 d\beta_2 \delta[\alpha_1 \beta_2 s - (\mathbf{k}_1 - \mathbf{k}_2)^2] = \frac{1}{s^3} \int \frac{d\alpha_1}{\alpha_1} = \frac{1}{s^3} \log \left(\frac{\alpha_{1 \max}}{\alpha_{1 \min}} \right) \approx \frac{1}{s^3} \log \left(\frac{s}{|t|} \right).$$

Note that the exact limits $\alpha_{1 \max}$ and $\alpha_{1 \min}$ are inessential when we care only about logarithmic contribution. After all calculations, we get the following two-loop result:

$$\text{Im } \mathcal{M}^{(2)} = \frac{m^6 g^6}{256 \pi^5 s} \log \left(\frac{s}{|t|} \right) \left[\int \frac{d^2 \mathbf{k}}{(\mathbf{k}^2 + m^2)((\mathbf{k} - \mathbf{q})^2 + m^2)} \right]^2 = \text{Im } \mathcal{M}^{(1)} x, \quad (22)$$

where

$$x = \frac{m^2 g^2}{16 \pi^3} \log \left(\frac{s}{|t|} \right) \int \frac{d^2 \mathbf{k}}{(\mathbf{k}^2 + m^2)((\mathbf{k} - \mathbf{q})^2 + m^2)}. \quad (23)$$

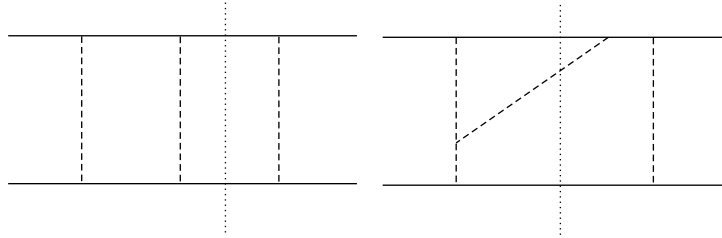


Fig. 8. Examples of two-loop diagrams which are suppressed for the toy model but are equally important in QCD

Before we move on, let us note that all other two-loop diagrams, for example, those shown in Fig. 8, are suppressed with respect to the ladder diagram, either by a power of s or due to absence of a logarithm. Note, however, that this is where our toy model is different from the true QCD, where such diagrams are equally important.

3.3. n -Loop Result. Consider now the n -loop ladder diagram, Fig. 9. The experience we gained in the previous cases allows us to expect that with each extra loop we get not only an extra g^2 factor but also an extra logarithm $\log(s/|t|)$, which comes from longitudinal integrals. In the transverse integrals, we do not expect to get any logarithmic enhancement.

The calculations confirm this expectation. The longitudinal integral

$$\int d\alpha_1 d\beta_1 \cdots d\alpha_n d\beta_n \delta(\ell_1^2) \cdots \delta(\ell_{n+1}^2)$$

gets the correct power of logarithms which come from the so-called *multi-Regge kinematics*

$$1 \gg \alpha_1 \gg \dots \gg \alpha_{n-1} \gg \alpha_n \approx \frac{|t|}{s}, \quad \frac{|t|}{s} \approx \beta_1 \ll \beta_2 \ll \dots \ll \beta_n \ll 1 \quad (24)$$

and is calculated as

$$\int_{|t|/s}^1 \frac{d\alpha_{n-1}}{\alpha_{n-1}} \int_{\alpha_{n-1}}^1 \frac{d\alpha_{n-2}}{\alpha_{n-2}} \cdots \int_{\alpha_3}^1 \frac{d\alpha_2}{\alpha_2} \int_{\alpha_2}^1 \frac{d\alpha_1}{\alpha_1} = \frac{1}{n!} \log \left(\frac{s}{|t|} \right)^n.$$

The transverse integrals are all of the same type as before. Therefore, we get the n -loop contribution to the leading logarithmic approximation:

$$\text{Im } \mathcal{M}^{(n)} = \text{Im } \mathcal{M}^{(1)} \frac{x^n}{n!} \quad (25)$$

with the same x as in (23).

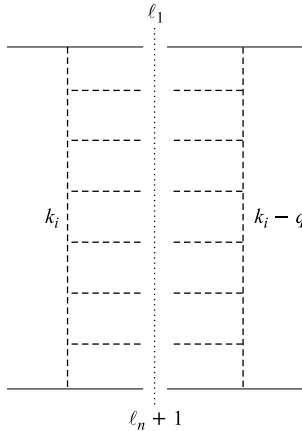


Fig. 9. Multiloop ladder diagram

3.4. Resumming All Loops. This simple form of the n -loop contribution allows us to resum all loops in the *leading logarithmic approximation*, that is, in the approximation in which we retain the largest (leading) kinematical logarithms for each order of perturbative expansion. The result is simply

$$\text{Im } \mathcal{M} = \text{Im } \mathcal{M}^{(1)} \left(1 + x + \frac{x^2}{2!} + \dots \right) = \text{Im } \mathcal{M}^{(1)} e^x. \quad (26)$$

Substituting x , we indeed obtain the Regge-like power law (11) with the intercept

$$\alpha_P(t) = -1 + \frac{g^2 m^2}{16\pi^3} \int \frac{d^2 \mathbf{k}}{(\mathbf{k}^2 + m^2)((\mathbf{k} - \mathbf{q})^2 + m^2)}. \quad (27)$$

Calculation of the remaining integral for nonzero \mathbf{q} is left for the reader. In particular,

$$\alpha_P(0) = -1 + \frac{g^2}{16\pi^2}. \quad (28)$$

This exercise illustrates how a noninteger exponent of energy can appear in diagrammatic calculations.

4. SOME FEATURES OF THE QCD POMERON

4.1. BFKL Theory. The perturbative QCD pomeron in the leading logarithmic approximation was derived by Balitsky, Fadin, Kuraev and Lipatov in 1976–1978 [9] and is known as the *BFKL pomeron*. The derivation was way more complicated than the simple scalar toy model explained above. In particular, in QCD there are nontrivial numerators for gluon couplings which requires additional diagrams to be taken into account. These diagrams are not strictly speaking of the ladder type, but using the trick of nonlocal Lipatov's vertices they can be rearranged in a way that looks like an effective ladder diagram. However, the t -channel gluons in these ladders are not bare but reggeized gluons; that is, they themselves are ladders with the gluon quantum numbers. Still, these complications were successfully overcome, and the resulting solution for the pomeron as the leading singularity with the vacuum quantum number exchange was found. A pedagogical introduction into these calculations can be found in the book [10] and lectures [11].

For fixed α_s the solution is not a Regge pole but a Regge cut. The edge of the cut, the leading singularity, has the intercept

$$\alpha_P(0) = 1 + \frac{4N_c \alpha_s}{\pi} \ln 2, \quad (29)$$

where $N_c = 3$ is the number of colors.

A decade ago the BFKL analysis was extended in the next-to-leading logarithmic approximation. This was a very long and complicated project, which culminated in the complete expression for the nonforward BFKL kernel at the next-to-leading logarithmic approximation [12]. As expected, the pomeron intercept was significantly reduced but was still noticeably above one.

4.2. Comparing with Phenomenology. This result caps an important theoretical achievement, but if one tries to apply it to the phenomenology, several uneasy questions emerge (an overview of this tension can be found in lectures [13]).

First, the intercept of the BFKL pomeron is too large. Taking, for example, $\alpha_s = 0.15$, one gets $\alpha_P \approx 1.4$, and $\sigma \propto s^{0.8}$. Thus, such a pomeron cannot explain the very slow energy growth which one observes in the total, elastic and diffractive cross sections. Inclusion of the next-to-leading logarithmic corrections relieves the tension a bit but does not completely cure this problem.

Even more disturbing is the fact that the dependence on hardness of the interaction is opposite to what we observe experimentally. Indeed, the softer the process, the larger is α_s , and the stronger is the energy growth according to the BFKL dynamics. But the data show a completely opposite trend.

The lesson that one learns here is that the BFKL result does not exhaust the full mechanism behind the pomeron. A better picture would be to think of the BFKL pomeron as the «hard» perturbative contribution to the pomeron exchange, and that there should exist a «soft» nonperturbative contribution with a very small or maybe even zero intercept. When the hardness of the pomeron-projectile vertex increases, the hard contribution becomes more

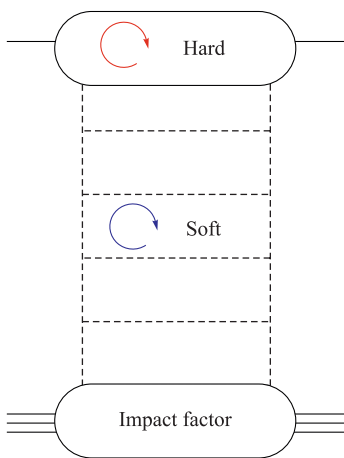


Fig. 10. The effective gluon ladder of the BFKL pomeron and two complications which arise in its phenomenological applications: the necessity to know the impact factors and the soft-hard diffusion

and more pronounced due to increased coupling to the projectile. This two-pomeron picture was popularized by Donnachie and Landshoff [14] who based their suggestion on pure phenomenological grounds, but it is also qualitatively supported by a more detailed analysis of the gluonic density in the proton [15].

There are additional obstacles which make application of the beautiful BFKL theory to the real world difficult if possible at all. First, the BFKL evolution equation allows one to understand the properties of the pomeron itself. If we want to calculate scattering of physical particles, for example protons, we need to couple the pomeron to them. Within the BFKL formalism, this coupling is described via impact factors, see Fig. 10. These impact factors are quite easy to calculate for fundamental particles (quarks, gluons, even photons), but they cannot be calculated perturbatively for protons. Therefore, a great deal of phenomenological modelling must be involved.

Another complication is related with the phenomenon called soft-hard diffusion [16]. The BFKL pomeron treats the gluons perturbatively, and for this assumption to be legitimate, one needs to assume that the typical gluon momenta in all loops from the top to the bottom of the ladder are large. Experimentally one can control only the uppermost or lowermost loops, for example, by studying processes induced by photons with very high virtuality. However, it turns out that even if the uppermost loop is hard, then the following loops becomes softer and softer. As a result, a fully developed ladder with several loops will still be dominated by the soft gluons in the middle. This is an intrinsic feature of the gluonic ladder and cannot be cured.

The third problem concerns the Froissart bound. Since the BFKL pomeron has an intercept strictly larger than 1, it would violate the Froissart bound at asymptotically large energies. It means that at such energies there must be a mechanism which slows down the energy growth of the cross sections.

One obvious possibility is to include multi-pomeron exchanges. However, the rigorous QCD calculations show that the situation is much more complicated than that. In fact, it seems now established that pomerons can directly interact with each other, merging or splitting or even producing intermediate pomeron loops in the t -channel. The details of this pomeron interaction are still the matter of hot debates. In the partonic language, the pomeron interactions lead to nonlinear evolution of the partonic densities and their eventual saturation. How to write these evolution equations in the most correct way, how to solve them, how they can be related with the observable phenomena, and do we really see the signals of saturation in the experimental data at the LHC, are among the issues on which no consensus is yet reached.

It seems that all these difficulties make the applicability of the BFKL formalism to the real processes very questionable, at least at the quantitative level. However, it does not mean the BFKL approach is of no use. Being a rigorous and exactly solvable feature of perturbative QCD, it plays the role of an «idealization» to which the true hadronic processes seem to tend. The qualitative features of the BFKL dynamics have become a very useful guide in understanding the real world semihard processes.

REFERENCES

1. Brower R. C. *et al.* The Pomeron and Gauge/String Duality // JHEP. 2007. V. 0712. P. 005.
2. White S. Diffraction at the LHC: A Non-technical Introduction. arXiv:1003.4252 [nucl-ex]; Ferro F. *et al.* Forward Physics at the LHC. arXiv:1012.5169 [hep-ex].
3. Fiore R. *et al.* Forward Physics at the LHC: Elastic Scattering // Intern. J. Mod. Phys. A. 2009. V. 24. P. 2551.
4. Anelli G. *et al.* (TOTEM Collab.). The TOTEM Experiment at the CERN Large Hadron Collider // JINST. 2008. V. 3. S08007.
5. Albrow M. G. *et al.* (FP420 R and D Collab.). The FP420 R&D Project: Higgs and New Physics with Forward Protons at the LHC // JINST. 2009. V. 4. T10001.
6. Ivanov I. P., Nikolaev N. N., Savin A. A. Diffractive Vector Meson Production at HERA: From Soft to Hard QCD // Phys. Part. Nucl. 2006. V. 37, Issue 1. P. 1.
7. Bourelly C., Soffer J., Wu T. T. Impact Picture Phenomenology for π^+p , K^+p , and pp , $\bar{p}p$ Elastic Scattering at High Energies // Eur. Phys. J. C. 2003. V. 28. P. 97.
8. Albrow M. G., Coughlin T. D., Forshaw J. R. Central Exclusive Particle Production at High Energy Hadron Colliders // Prog. Part. Nucl. Phys. 2010. V. 65. P. 149.
9. Kuraev E. A., Lipatov L. N., Fadin V. S. Multi-Reggeon Processes in the Yang–Mills Theory // ZhETF. 1976. V. 71. P. 840; Kuraev E. A., Lipatov L. N., Fadin V. S. The Pomeron Singularity in Non-Abelian Gauge Theories // ZhETF. 1977. V. 72. P. 377; Balitsky I. I., Lipatov L. N. The Pomeron Singularity in Quantum Chromodynamics // Yad. Fiz. 1978. V. 28. P. 1597.
10. Forshaw J., Ross D. Quantum Chromodynamics and the Pomeron // Cambridge Lect. Notes Phys. 1997. V. 9. P. 1.

11. *Del Duca V.* An Introduction to the Perturbative QCD Pomeron and to Jet Physics at Large Rapidities. arXiv:hep-ph/9503226.
12. *Fadin V. S., Fiore R.* Non-forward NLO BFKL Kernel // *Phys. Rev. D.* 2005. V. 72. P. P.014018.
13. *Levin E.* An Introduction to Pomerons. hep-ph/9808486.
14. *Donnachie A., Landshoff P. V.* Small x : Two Pomerons! // *Phys. Lett. B.* 1998. V. 437. P. 408.
15. *Ivanov I. P., Nikolaev N. N.* Anatomy of the Differential Gluon Structure Function of the Proton from the Experimental Data on $F(2p)(x, Q_2)$ // *Phys. Rev. D.* 2002. V. 65. P. 054004.
16. *Bartels J., Lotter H.* A Note on the BFKL Pomeron and the «Hot Spot» Cross-Section // *Phys. Lett. B.* 1993. V. 309. P. 400;
Ciafaloni M. et al. Tunneling Transition to the Pomeron Regime // *Phys. Lett. B.* 2002. V. 541. P. 314.

Received on November 30, 2013.